Journal of Experimental Botany, Vol. 67, No. 6 pp. 1731–1743, 2016
doi:10.1093/jxb/erv564 Advance Access publication 21 January 2016

RESEARCH PAPER

The Arabidopsis microtubule-associated protein MAP65-3 supports infection by filamentous biotrophic pathogens by down-regulating salicylic acid-dependent defenses

Michaël Quentin[1,*], Isabelle Baurès[1,*], Caroline Hoefle[2,*], Marie-Cécile Caillaud[3,†], Valérie Allasia[1], Franck Panabières[1], Pierre Abad[1], Ralph Hückelhoven[2], Harald Keller[1,‡] and Bruno Favery[1,‡]

[1] INRA, Université de Nice Sophia Antipolis, CNRS, UMR 1355-7254 Institut Sophia Agrobiotech, 06900 Sophia Antipolis, France
[2] Lehrstuhl für Phytopathologie, Technische Universität München, D-85350 Freising-Weihenstephan, Germany
[3] The Sainsbury Laboratory, John Innes Centre, Norwich Research Park, Norwich NR4 7UH, UK

* These authors contributed equally to this work.
† Present address: CNRS, INRA, ENS Lyon, Université Claude Bernard Lyon 1, Laboratoire de Reproduction et Développement des Plantes, Université de Lyon, 46 Allée d'Italie, 69364 Lyon Cedex 07, France.
‡ Correspondence: favery@sophia.inra.fr or keller@sophia.inra.fr

Received 6 October 2015; Accepted 16 December 2015

Editor: Katherine Denby, University of Warwick

Abstract

The oomycete *Hyaloperonospora arabidopsidis* and the ascomycete *Erysiphe cruciferarum* are obligate biotrophic pathogens causing downy mildew and powdery mildew, respectively, on Arabidopsis. Upon infection, the filamentous pathogens induce the formation of intracellular bulbous structures called haustoria, which are required for the biotrophic lifestyle. We previously showed that the microtubule-associated protein AtMAP65-3 plays a critical role in organizing cytoskeleton microtubule arrays during mitosis and cytokinesis. This renders the protein essential for the development of giant cells, which are the feeding sites induced by root knot nematodes. Here, we show that *AtMAP65-3* expression is also induced in leaves upon infection by the downy mildew oomycete and the powdery mildew fungus. Loss of *AtMAP65-3* function in the *map65-3* mutant dramatically reduced infection by both pathogens, predominantly at the stages of leaf penetration. Whole-transcriptome analysis showed an over-represented, constitutive activation of genes involved in salicylic acid (SA) biosynthesis, signaling, and defense execution in *map65-3*, whereas jasmonic acid (JA)-mediated signaling was down-regulated. Preventing SA synthesis and accumulation in *map65-3* rescued plant susceptibility to pathogens, but not the developmental phenotype caused by cytoskeleton defaults. AtMAP65-3 thus has a dual role. It positively regulates cytokinesis, thus plant growth and development, and negatively interferes with plant defense against filamentous biotrophs. Our data suggest that downy mildew and powdery mildew stimulate *AtMAP65-3* expression to down-regulate SA signaling for infection.

Key words: Cytoskeleton, fungus, microtubules, mildew, oomycete, plant defense, salicylic acid.

Introduction

The microtubule (MT) cytoskeleton is a highly flexible and dynamic polar structure of the plant cell, assembled from tubulin heterodimers. It is involved in nuclear and cell division, in cell morphogenesis and expansion, and in intracellular transport (Wasteneys and Galway, 2003; Wasteneys, 2004; Hamada, 2014). MTs also play a role in plant responses to biotic and abiotic stress exposure, and their rearrangements accompany both defense and successful infection by symbiotic and pathogenic microbes (Schmidt and Panstruga, 2007; Hardham, 2013). MT re-arrangements occur during arbuscular mycorrhizal (Genre *et al.*, 2005) and rhizobial symbiosis (Vassileva *et al.*, 2005), during the formation of plant parasitic nematode feeding sites (Caillaud *et al.*, 2008*a*; de Almeida Engler and Favery, 2011), following virus attack (Martinière *et al.*, 2009), or following infection by filamentous oomycetes or fungi (Kobayashi *et al.*, 1994; Baluska *et al.*, 1995; Cahill *et al.*, 2002; Takemoto *et al.*, 2003; Hardham *et al.*, 2008; Hoefle *et al.*, 2011). Microtubule-associated proteins (MAPs) and their regulatory kinases and phosphatases are instrumental for microtubule dynamics (Wasteneys, 2004; Gardiner, 2013; Hamada, 2014). They, and the small Rho of Plants (ROP) GTPases that regulate the MT cytoskeleton (Mucha *et al.*, 2011), have been shown to determine plant susceptibility to viruses and fungi (Kragler *et al.*, 2003; Ouko *et al.*, 2010; Hoefle *et al.*, 2011; Poraty-Gavra *et al.*, 2013). We previously identified the *Arabidopsis thaliana* MAP65-3 (AtMAP65-3) as a critical module for root-knot nematode-induced feeding, giant cell ontogenesis, and for successful pathogen development (Caillaud *et al.*, 2008*b*).

Plant MAP65s are involved in the spatially and temporally regulated binding and bundling of MTs (Chan *et al.*, 1999; Hamada, 2014). In *A. thaliana*, nine members of this family were identified (Hussey *et al.*, 2002) and individual members have particular functions with respect to different MT arrays. AtMAP65-3 is only associated with mitotic MT arrays (Müller *et al.*, 2004; Caillaud *et al.*, 2008*b*; Ho *et al.*, 2011). Here, the protein organizes both spindle morphogenesis and phragmoplast expansion (Müller *et al.*, 2004; Caillaud *et al.*, 2008*b*; Ho *et al.*, 2011). Consequently, AtMAP65-3 loss-of-function mutants are dwarf, with both shoots and roots being stunted, and polynucleate, hypertrophied cells with aberrant cell wall stubs occur frequently (Müller *et al.*, 2004; Caillaud *et al.*, 2008*b*; Ho *et al.*, 2011).

Plants protect themselves against pathogenic microorganisms by combining constitutive and induced defense mechanisms. The induction of plant defenses involves the recognition of compounds derived from the pathogen, called pathogen-associated molecular patterns (PAMPs). Pattern-triggered immunity (PTI) results from PAMP perception, which leads to the activation of signaling cascades, and the subsequent induction of defense-related genes (Zipfel *et al.*, 2004; Jones and Dangl, 2006). Pathogens are able to suppress these defenses by secreting effector proteins that manipulate host cell functions. In turn, plants evolved resistance proteins, which allow recognition of these effectors or their activities. This leads to effector-triggered immunity (ETI) and activation of the hypersensitive response (HR). The HR involves local programmed cell death that prevents pathogen spreading within the plant (Zipfel *et al.*, 2004; Jones and Dangl, 2006). Both PTI and ETI/HR involve mitogen-activated protein kinase (MAPK) cascades, the production of reactive oxygen species (ROS), and the transcriptional activation of genes, which, among others, encode antimicrobial pathogenesis-related (PR) proteins. The signaling pathways of PTI or ETI are fine-tuned by plant signaling molecules such as salicylic acid (SA), jasmonic acid (JA), and ethylene (ET) (Glazebrook, 2005; Pieterse *et al.*, 2012).

The hormone SA plays a major role in plant resistance to (hemi-)biotrophic pathogens (Pieterse *et al.*, 2012). In *A. thaliana*, SA synthesis occurs in plastids via isochorismate synthase 1 (ICS1 or SID2) and is triggered by pathogens. SA can be exported to the cytosol by the transporter enhanced disease susceptibility 5 (EDS5). SA accumulated in the cytoplasm can be converted to SA glucoside (SAG), which is stored in the vacuole and hydrolyzed back to SA when needed. Elevated levels of total SA (free SA plus SAG) have been correlated with the induction of defense gene expression and enhanced plant resistance (Pieterse *et al.*, 2012). In addition, SA is a key regulator of plant immunity through its antagonistic interaction with ET and JA pathways (Glazebrook, 2005). Different from SA, JA and ET accumulate mainly in response to necrotrophic pathogens.

An increasing number of mutants with reduced susceptibility to plant pathogens are described, and breeding for loss of susceptibility becomes a new strategy to achieve disease resistance (de Almeida-Engler *et al.*, 2005; Dangl *et al.*, 2013; Hückelhoven *et al.*, 2013). Loss of disease susceptibility is frequently caused by a deregulation of SA- or JA-dependent plant defense signaling, by the impairment of cellular rearrangements, or by the limitation of nutrient supply for the pathogen (Dangl *et al.*, 2013; Hückelhoven *et al.*, 2013; Lapin and Van den Ackerveken, 2013; Van Schie and Takken, 2014).

In this study, we show that expression of the gene encoding AtMAP65-3 is strongly induced in *A. thaliana* upon infection by two biotrophic filamentous pathogens, the oomycete *Hyaloperonospora arabidopsidis* (*Hpa*) and the powdery mildew fungus *Erysiphe cruciferarum* (*Ec*). Both pathogens develop haustoria inside host cells that constitute the feeding structures for nutrient supply (O'Connell and Panstruga, 2006). We show that plants mutated in *AtMAP65-3* are impaired in their susceptibility to both filamentous pathogens. Mutants accumulate increased levels of SA, and constitutively express genes encoding PR proteins in the leaves. Increased SA accumulation is not responsible for the mutant dwarfism, indicating that AtMAP65-3 exerts a dual role in positively regulating plant growth and development, and in negatively regulating plant defense responses.

Materials and methods

Plant material and growth conditions

Arabidopsis lines used for the experiments were from the Wassilewskija (WS-4) and Columbia (Col-0) wild-type (Wt) genetic background. The *map65-3* T-DNA mutant (*dyc283*), the complemented line *Cpmap65-3* (*map65-3* expressing the *AtMAP65-3* gene under the control of its native promoter), and plants expressing the β-glucuronidase (GUS) reporter gene under the control of the *AtMAP65-3* promoter have been described previously (Caillaud *et al.*, 2008*b*). Arabidopsis plants expressing the GFP–TUA6 (green fluorescent protein-tagged α-tubulin) (Ueda *et al.*, 1999) and *sid2.1* mutant were used (Nawrath and Métraux, 1999). For *in vitro* culture, plants were grown in growth chambers at 20 °C with a 12 h photoperiod on Murashige and Skoog (MS) medium (Duchefa Biochemie), supplemented with 1% sucrose and 0.7% plant cell culture-tested agar (Sigma Aldrich). When necessary, 15-day-old plants were further transferred to soil and grown in growth chambers at 22 °C under a 16 h day/8 h dark photoperiod. For pathogen assays with *Ec*, plants were grown directly on soil at 22 °C, 65% relative humidity, and a 10 h day/14 h dark photoperiod for 4–5 weeks before inoculation.

Transgenic plants, crossings, and genotyping

The vector carrying the *35S::NahG* construct (Delaney *et al.*, 1994) was transformed via *Agrobacterium tumefaciens* strain GV3101 into homozygous *map65-3* Arabidopsis plants using the dipping method (Clough and Bent, 1998), and selected on MS medium containing 5 mg l^{-1} phosphinothricine. Transformed plants were transferred to soil, and seeds were collected. For each construct, 10 independent primary T_1 transformants were verified by PCR, and T_2 plants were obtained for subsequent analysis. To eliminate SA completely from *map65-3* while minimizing catechol-related NahG effects, plants homozygous for the *map65-3* mutation with *NahG* were crossed with the *sid2.1* mutant. The *map65-3* plants were also crossed with the GFP–TUA6 transgenic line. For T_2 progeny genotyping, genomic DNA extraction and PCR amplifications were performed using the REDExtract-N-Amp™ Plant PCR Kit (Sigma) according to the manufacturer's instructions. For genotyping the *sid2.1* mutation, *SID2* amplicons obtained from genomic DNA were digested with *Mse*I, allowing discrimination of homozygous mutant lines as described elsewhere (Nawrath and Métraux, 1999). The TUA6 lines were further selected for expression of the fluorescent marker. Primers used for genotyping are listed in Supplementary Table S1 at *JXB* online.

Pathogen assays

The *Hpa* isolates Emwa1 and Waco9 were transferred weekly onto the genetically susceptible Arabidopsis accessions WS (Emwa1 and Waco9) or Col-0 (Waco9). Plants were cultivated on soil in growth chambers at 16 °C with a 12 h photoperiod, and infections and pathogenicity assays were performed as described previously (Quentin *et al.*, 2009; Caillaud *et al.*, 2012). Arabidopsis plants were infected with *Ec* as described previously (Hoefle *et al.*, 2011). Susceptibility to *Ec* was scored by visual examination 7, 9, and 11 days after inoculation (dai). Plants were distributed in three categories of susceptibility with 0–30%, 30–60%, and >60% diseased leaf area.

Histological analysis

GUS activity was analyzed histochemically as described (Quentin *et al.*, 2009). To monitor progression of plant infection by *Hpa*, cotyledons or young leaves of Arabidopsis were fixed in 1% glutaraldehyde (v/v), 4% (v/v) formaldehyde in phosphate buffer 0.1 M, pH 7 and de-stained in an ethanol dilution series. Finally, the autofluorescence of the oomycete was visualized with a confocal microscope (excitation 488 nm). Lactophenol–trypan blue staining of *Hpa* was performed, on tissue fixed as described above, according to Parker *et al.* (1997). For callose visualization, infected tissues were fixed as described above, bleached in a series of increasing ethanol concentration, and stained with 0.005% aniline blue in 0.07 M sodium phosphate buffer pH 7.2 (w/v) before observation under an Axioplan fluorescent microscope (Zeiss). Images were acquired with a Zeiss AxioCam camera and analyzed with Zeiss Axiovision digital image-processing software, version 4.4.

For microscopic analysis of the powdery mildew development, leaves were harvested 48 hours after infection (hai), bleached in ethanol/acetic acid (6:1, v/v), and fungal structures were stained with acetic/blue ink (15% acetic acid/blue ink 9:1, v/v).

Confocal laser scanning microscopy

High-resolution images of GFP fluorescence, and of autofluorescence of oomycete hyphae, were obtained with a confocal laser scanning microscope (Axiovert 200 M, LSM510 META, Zeiss, Jena, Germany; or Leica SP5, Leica, Mannheim, Germany). GFP was excited with an argon laser at 488 nm, and fluorescence was recorded in a window ranging from 505 nm to 530 nm. Confocal images were processed using the Zeiss LSM Image Browser or Leica Application Suite.

RNA isolation and quantitative real-time PCR (qRT-PCR) analysis

Infected and non-infected plantlets were harvested, frozen in liquid nitrogen, and stored at –80 °C until use for RNA extraction. Total RNA was extracted from *A. thaliana* seedlings using TRIZOL Reagent (Invitrogen) following the instructions of the manufacturer. DNA was degraded using RNase-free DNase from Ambion. A 1 µg aliquot of RNA was reverse transcribed using the iScript cDNA Synthesis Kit (Biorad). Amplification and detection were performed in the Opticon 2 system (MJ research Biorad). Reactions were in a final volume of 15 µl containing 10 µl of qPCR MasterMix Plus For SYBRGreen I No Rox (Eurogentec), 0.5 mM of each primer, and 8 ng of cDNA template. PCR conditions were as follows: 95 °C for 15 min, followed by 40 cycles of 95 °C for 15 s, 56 °C for 30 s, and 72 °C for 30 s. At the end of the program, a melting curve (from 60 °C to 95 °C, read every 0.5 °C) was determined to ensure that only single products were formed. *Ubiquitin-specific protease 22* (*UBP22*, *At5g10790*) and *Oxidase Assembly 1* (*OXA1*, *At5g62050*) expression was used to normalize the transcript level in each sample (Quentin *et al.*, 2009). Raw data were treated using the MJ OpticonMonitor Analysis software (version 3.1, Biorad). Relative quantifications were made with the modified ΔCt method employed by the qBase 1.3.5 software. qBase was also used to determine the stability of reference genes. Coefficients of variation of 32.65% and 27.34% for *OXA1* and *UBP22*, respectively, as well as geNorm stability M-values of 0.8487 for both genes indicated stable expression under our experimental conditions (Hellemans *et al.*, 2007). Primers used for qRT-PCR analyses are listed in Supplementary Table S1.

Microarray and microarray data analysis

For whole-genome transcript profiling, RNA from cotyledons of the different lines and from two independent biological replicates was extracted 3 d after water treatment or *Hpa* inoculation, and submitted to analysis on Affymetrix ATH1 arrays, which were operated by the NASC Affymetrix service. Background adjustment, quantile normalization, and probe set summarization were performed with the Affymetrix Power Tools APT1.14.4 software package. Normalized data obtained for all probe sets were then compared, and $\log_2$ ratios from all comparisons were submitted to a replicate control. Values were considered as not being relevant when the difference between replicate ratios was higher than 0.75% of the mean $\log_2$ ratio, and were eliminated. Gene expression was considered as being different between treatments and backgrounds when mean $\log_2$ signal ratios were ≥1 or ≤ –1. The functional classification of the genes was performed according to the tair10 Gene Ontology (GO). Over-representation of GO terms was analyzed using the VirtualPlant 1.3 Online analysis tool at www.virtualplant.org (Katari *et al.*, 2010). Data from the transcriptome analyses were deposited at the Gene Expression Omnibus database (http://www.ncbi.nlm.nih.gov/geo/) and assigned the identifier GSE73351.

SA quantification

SA was extracted from three independent biological replicates of 10-day-old Wt, *map65-3*, and *Cpmap65-3* seedlings, 4 d after treatment with water or *Hpa*, and quantified according to Meuwley and Metraux (1993) with some modifications. Briefly, harvested seedlings were ground in a mortar under liquid N_2, and tissue powder corresponding to 250 mg FW was extracted with 1 ml of ethanol containing 300 ng of *o*-anisic acid as internal standard. After centrifugation for 5 min at 10 000 *g*, the supernatant was recovered and the pellet re-extracted with 2 ml of aqueous methanol (90% v/v). After centrifugation, the supernatants from both extractions were pooled and the volume was reduced in a Speed Vac concentrator to 50 µl, before 500 µl of ethyl acetate:cyclohexane (1:1, v/v) and 200 µl of trichloroacetic acid (5%, w/v) were added. The mixture was vortexed for 30 s and centrifuged at 10 000 *g* for 5 min. The aqueous phase was re-extracted with 500 µl of ethyl acetate:cyclohexane (1:1, v/v). The aqueous and the organic fractions from both extractions were pooled. The organic fraction containing non-conjugated SA was brought to dryness in a Speed Vac concentrator and resuspended in 100 µl of aqueous methanol (10%, v/v) supplemented with 0.1% trifluoroacetic acid (v/v). The aqueous fraction was hydrolyzed in 4 M HCl at 80 °C for 1 h, supplemented with the internal standard, and submitted to organic solvent extraction, concentration, and resuspension, as described above. All samples were separated on an Inertsil 5OD53 C_{18} column (5 µm, 250 × 4.6 mm i.d.; Interchim, Montlucon, France) in a linear methanol gradient from 10% to 82% aqueous methanol (v/v) over 30.4 min, using a Shimazu LC20A HPLC system with fluorometric detection (excitation at 305 nm; emission at 407 nm and 365 nm for SA and *o*-anisic acid, respectively). The quantities were determined with a standard curve established for authentic SA (Sigma).

Results

Infection with Hpa *and* Ec *stimulates transcription of* AtMAP65-3 *in Arabidopsis*

The expression profile of *AtMAP65-3* was analyzed using transgenic plants expressing the GUS reporter gene under the control of the *AtMAP65-3* promoter (Caillaud *et al.*, 2008b). In 2-week-old plantlets, GUS staining was not observed in non-infected cotyledons (Fig. 1A). At 4 dai with *Hpa*, GUS staining was observed in cells from cotyledons and young leaves that were in contact with the growing hypha (Fig. 1B, C). This localization of *AtMAP65-3* expression appeared to be restricted to cells harboring haustoria (Fig. 1D). In contrast to intercellular growing hyphae of *Hpa*, the mycelium of *Ec* does not enter the plant tissues, but remains on the leaf surface, driving haustoria into epidermis cells. When rosette leaves from plants of the *AtMAP65-3* reporter line were inoculated with *Ec* conidia, GUS activity was revealed at veins, 16–48 hai (Fig. 1F). No staining was observed in non-infected rosette leaves (Fig. 1E). In cotyledons and leaves, *AtMAP65-3* is thus stimulated by infection with both mildews.

Absence of AtMAP65-3 reduces susceptibility to filamentous biotrophs

To investigate further the contribution of AtMAP65-3 to the interaction between Arabidopsis and *Hpa*, *map65-3* mutants (Caillaud *et al.*, 2008*b*) and Wt plants (ecotype WS) were inoculated with the *Hpa* isolate Emwa1. According to the general criterion for analyzing plant susceptibility and resistance to *Hpa* (Kwon *et al.*, 2008), we determined the asexual sporulation rates at 7 dai. We found that *map65-3* was significantly less susceptible to *Hpa* than the Wt, and that sporulation was reduced by ~50% on the *map65-3* mutants (Fig. 2A). This decreased susceptibility phenotype was fully complemented by expressing *AtMAP65-3* in the *map65-3* mutant background (*Cpmap65-3* line; Caillaud *et al.*, 2008b; Fig. 2A). Our data thus indicate that AtMAP65-3 contributes

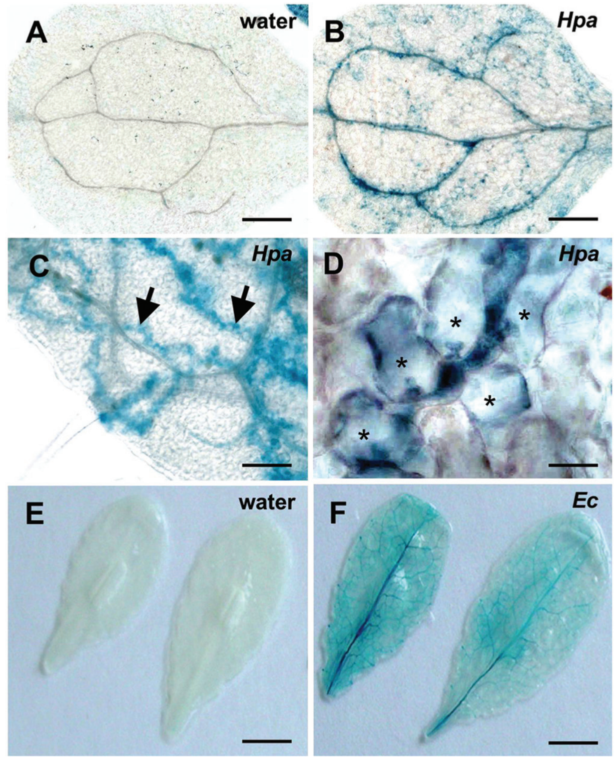

Fig. 1. Expression of *AtMAP65-3* during the interaction with *H. arabidopsidis* and *E. cruciferarum*. (A, B) GUS expression in cotyledons from an *A. thaliana* line harboring a fusion between the *AtMAP65-3* promoter and the GUS reporter gene treated with water (A) or inoculated with *Hpa* 4 dai (B). (C, D) Promoter activation is restricted to a small number of young leaf cells in close contact with invading hyphae (C; arrows), especially in haustoria-harboring cells (D; asterisks). (E, F) GUS expression in leaves from the *AtMAP65-3* promoter GUS line treated with water (E) or inoculated with *Ec* (F). Scale bars=600 µm (A and B), 100 µm (C), 20 µm (D), and 4 mm (E and F).

to downy mildew susceptibility of Arabidopsis, and that its absence increases resistance.

We further analyzed whether the infection-responsive transcription of *AtMAP65-3* upon inoculation with *Ec* reflects a role in the interaction with powdery mildew. We challenged plants from the Wt and the *map65-3* mutant line with *Ec* conidia, and analyzed macroscopic disease symptoms from 7 to 11 dai (Fig. 2B). The *map65-3* mutant appeared visibly more resistant to the fungus than the Wt. On the mutant, disease extended to <30% of infected leaf areas in >70% of all inoculated plants. In contrast, the leaves of >70% of the Wt plants presented disease symptoms that covered areas between 30% and 100% of total leaf surfaces (Fig. 2B).

The map65-3 *mutation does not affect haustoria-mediated structural rearrangements in host cells*

AtMAP65-3 binds and bundles MTs. We thus suspected that the observed up-regulation of *AtMAP65-3* upon infection with *Hpa* and *Ec* might reflect a role for the protein in organizing MTs during compatible interactions with filamentous pathogens. To verify this hypothesis, we inoculated *Hpa* on plants from a transgenic Arabidopsis line expressing

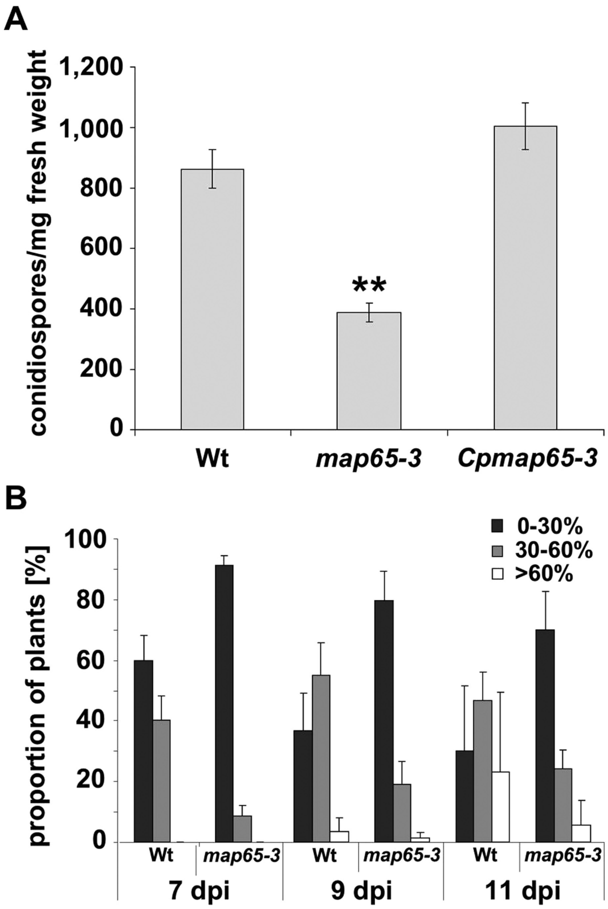

Fig. 2. The expression of *AtMAP65-3* determines susceptibility of Arabidopsis to biotrophic filamentous pathogens. (A) *Hpa* conidiospore production on cotyledons from the Wt (WS), from the *map65-3* mutant, and from a complemented line (*Cpmap65-3*). Data represent means ±SE for 20 samples. Asterisks indicate a significant difference (*t*-test, $P<0.01$). This experiment was conducted three times with similar results. (B) Disease symptoms on rosette leaves from the Wt (WS) and the *map65-3* mutant upon infection with *Ec*. Disease symptoms were scored after visual inspection of the whole plant 7, 9, and 11 dai. Infected leaves were classified in three categories with <30%, 30–60%, and >60% of diseased leaf areas. Data are means ±SD from three independent biological replicates, each composed of the analysis of 10 individual plants.

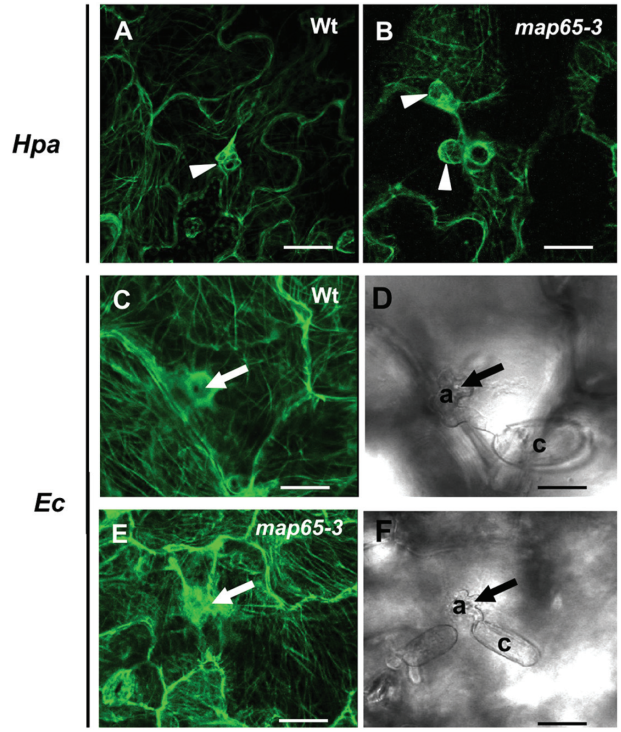

Fig. 3. Knocking out *AtMAP65-3* does not affect microtubule rearrangements that are associated with *Hpa* haustoria development and *Ec* penetration. (A, B) GFP-labelled MTs embed *Hpa*-induced haustoria (arrowhead) in cotyledon mesophyll cells from both the Wt (A) and the *map65-3* mutant (B). (C–F) GFP-labeled MT rearrangements at the *Ec* infection site (arrows) in epidermal cells of the Wt (C) and the *map65-3* mutant (E). (D) and (F) Bright-field images corresponding to confocal images (C) and (E), respectively, and showing *Ec* conidium (c) and appressorium (a) on the epidermal cell surface. MTs were observed by confocal microscopy in transgenic Arabidopsis plants expressing GFP-tagged α-tubulin 6 (GFP–TUA6) in the Wt or *map65-3* backgrounds. Scale bars=15 µm (A and B), 13 µm (C–F). (This figure is available in colour at *JXB* online.)

GFP-tagged α-tubulin 6 (GFP–TUA6) (Ueda *et al.*, 1999), and from a cross between this line and the *map65-3* mutant. MT arrays in cells harboring haustoria were then analyzed using *in vivo* confocal microscopy. As in non-inoculated plants, GFP–TUA6 fluorescence was associated with cortical MT arrays in epidermal cells from cotyledons and leaves. In *Hpa* haustoria-bearing cells, rearrangements of MTs occurred and were reflected by an accumulation of the GFP signal at haustoria. Subsequently, thick MT arrays encircled the haustoria (Figs 3A, B). MT arrays were also observed extending from the cell cortex towards the haustoria of *Hpa* (Fig. 3A). We did not find obvious differences in MT organization around haustoria between *Hpa*-inoculated Wt and *map65-3* mutant plants (Figs 3A, B). Upon inoculation with *Ec*, we observed either areas of reduced GFP–TUA6 signal intensities or a diffuse fluorescence of GFP–TUA6 at sites below appressorium formation by *Ec* between 16 h and 24 h after inoculation (Fig. 3C). However, we did not observe any obvious differences between the Wt (Fig. 3C) and the *map65-3* mutant (Fig. 3E), when comparing the patterns of GFP–TUA6 signals at *Ec* penetration sites.

We further analyzed the morphology of hypha and haustoria from *Hpa*, which colonizes either the Wt or the *map65-3* mutant. Plants were inoculated and autofluorescence of the oomycete was visualized at 4 dai using a confocal microscope. In both Wt and *map65-3* plants, *Hpa* hyphae developed intercellularly once the oomycete had entered the cotyledon, branched, and formed haustoria inside host cells. Confocal microscopy showed that haustoria exhibited a characteristic shape with no obvious difference between the Wt and *map65-3* plants (Supplementary Fig. S1).

MTs also participate in the deposition of callose in Arabidopsis cells (Cai *et al.*, 2011). Callose biosynthesis and deposition is a typical plant defense response aimed at reinforcing the cell wall as a physical barrier against penetration (Ellinger and Voigt, 2014). However, both *Hpa* and *Ec* require the deposition of callose around the haustorial neck as a scaffold for stabilizing haustoria, and thus for successful infection (Jacobs *et al.*, 2003; Nishimura *et al.*, 2003). The *map65-3*

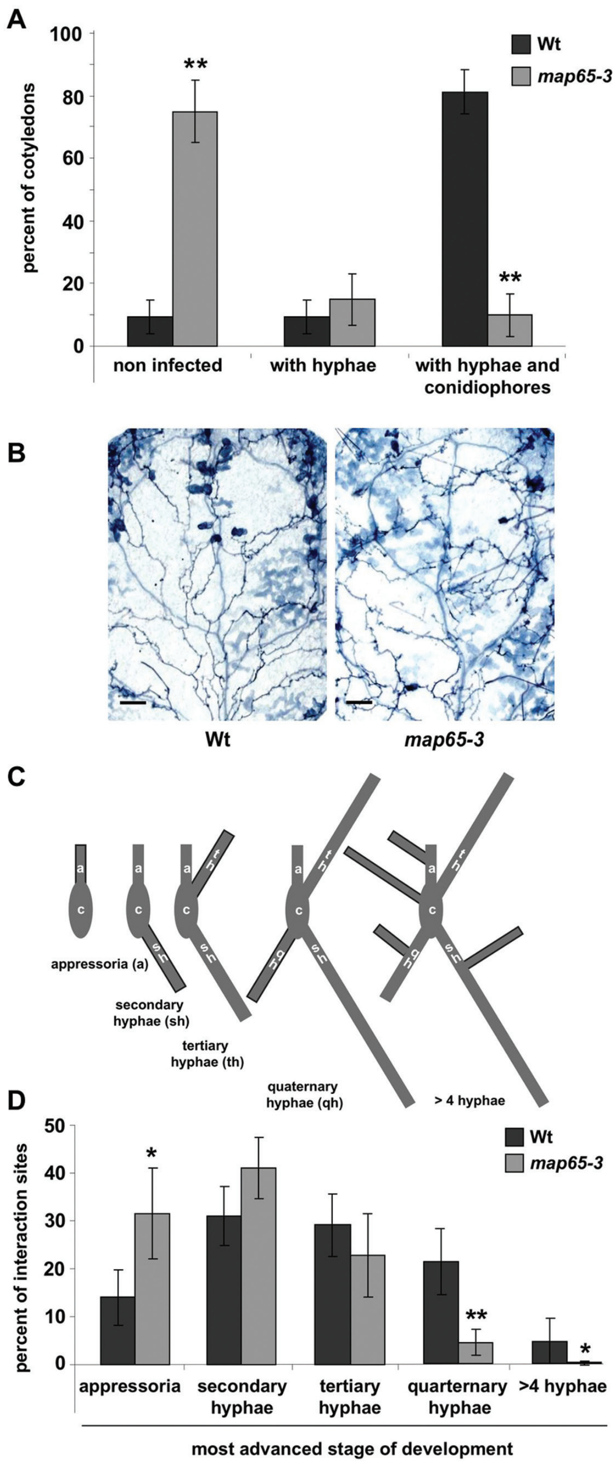

Fig. 4. *AtMAP65-3* regulates pathogen entry into Arabidopsis tissues. (A) The presence of hyphae and/or conidiophores was scored in cotyledons (n=20) stained with trypan blue 7 dai with *Hpa*. Asterisk indicates a significant difference between the Wt and the *map65-3* mutant (t-test, P<0.01). (B) Hyphal network stained with trypan blue in cotyledons of the Wt and the *map65-3* mutant, 7 dai with *Hpa*. Scale bars=200 µm. (C, D) Analysis of individual interaction sites on each rosette leaf (n=10) inoculated with *Ec* revealed differences in the penetration success and fungal development on the first epidermal pavement cell 48 hai. (C) Sketch explaining the analysis. For single interaction sites, the most advanced stage of fungal development, beginning from individual conidia (c), was scored. (D) Percentage of total infection sites that were stacked at different stages between appressoria (a) formation and the development of higher order (>4) hyphae. Data are means ±SE. Asterisks indicate a significant difference between the Wt and the *map65-3* mutant (t-test; ** P <0.01; * P<0.05).

mutation had no effect on the typical callose ring deposition at the neck of *Hpa* haustoria, as confirmed using aniline blue staining and fluorescent microscopy (Supplementary Fig. S1).

AtMAP65-3 determines the penetration efficiency of Hpa *and* Ec

A notable phenotype we observed was that penetration efficiency of the filamentous pathogens was strongly reduced on *map65-3* plants. *Hpa* spores germinate on leaf surfaces and form appressoria, enabling infection pegs to overcome the cuticle. Once inside the leaf, the intercellularly growing hyphae branch, and establish an expanding network. The infection cycle is achieved with the formation and subsequent propagation of asexual conidiospores through stomatal openings (Koch and Slusarenko, 1990). To identify which stage of the *Hpa* infection cycle is impacted by AtMAP65-3, infected cotyledons from the Wt and the mutant were stained with trypan blue at 4 dai and scored for the presence of intercellular hyphae and the production of conidiophores. About 80% of inoculated cotyledons from the *map65-3* mutant did not present intercellular hyphae and conidiophores (i.e. no symptoms of infection), whereas only 10% of cotyledons from the Wt were free from *Hpa* (Fig. 4A). In contrast, only 10% of *map65-3* cotyledons contained hyphae undergoing sporulation, whereas *Hpa* was completing the infection cycle in ~80% of Wt cotyledons (Fig. 4A). The mutants thus exhibited a significantly higher proportion of uninfected tissues. However, cotyledons that were successfully infected contained hyphal networks of similar appearance in the Wt and the mutant (Fig. 4B). These findings indicate that AtMAP65-3 determines oomycete penetration into plant tissues.

The *map65-3* mutant plants also exhibited enhanced penetration resistance to the powdery mildew fungus. *Ec* conidia germinate on the plant surface, and host penetration depends on the formation of an appressorium and a penetration peg, allowing the physical barrier of wax, cuticle, and cell wall to be overcome. The fungus then forms haustoria in intact epidermal cells that constitute sinks for water, minerals, and nutrients, allowing further hyphal growth on the cuticular surface (O'Connell and Panstruga, 2006). Microscopic inspections showed that powdery mildew succeeded better in establishing a compatible interaction on the Wt than on the *map65-3* plants. *Ec* formed significantly fewer high-order hyphae (≥4), 48 h after inoculation, on leaves from the mutant than on those from the Wt (Fig. 4C). This observation is indicative of reduced success in fungal establishment. Congruently, we observed a significant increase in the number of appressoria without formation of epicuticular hyphae on leaf surfaces of *map65-3*. This observation is indicative of failed powdery mildew attempts to penetrate rosette leaves (Fig. 4C).

Taken together, our observations strongly suggest that AtMAP65-3 exerts a function which favors the penetration of filamentous biotrophs into leaves and cotyledons.

Absence of AtMAP65-3 primes Arabidopsis for SA-dependent defenses

The decreased infection success on *map65-3* mutants might result either from a gain of resistance or from a loss of

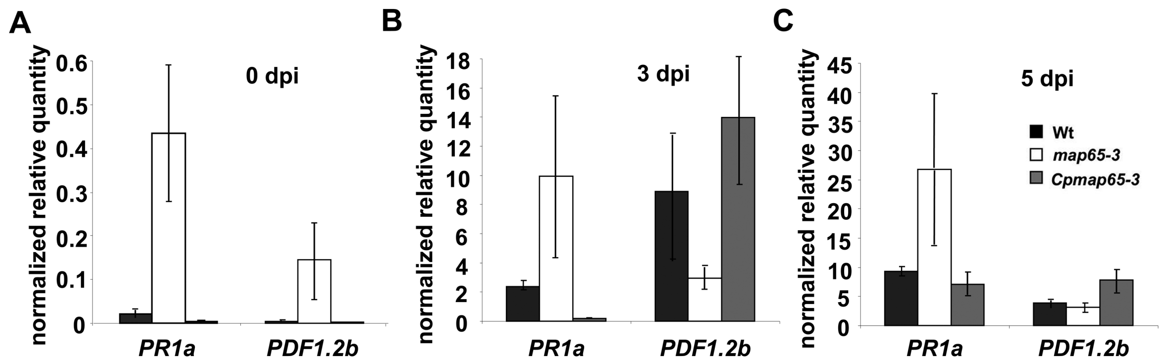

Fig. 5. The *map65-3* mutant shows constitutive expression of defense-related genes in shoots. (A–C) Relative gene expression of *PR1* and *PDF1.2b* in shoots of Wt, *map65-3* plants, and the *Cpmap65-3* complemented line at 0, 3, or 5 dai with *Hpa*. qRT-PCR was performed with *PR1* and *PDF1.2b* gene-specific primers, and expression levels were normalized to the reference genes *UBP22* and *OXA1*. Data are means ±SE from three biological replicates.

susceptibility. To test this, we first compared the expression levels of the defense-related genes *PR1* and *PDF1.2b* between plants from the *map65-3* mutant and the Wt. *PR1* and *PDF1.2b* are common markers for activated SA- and JA-dependent defense signaling pathways, respectively (Pieterse *et al.*, 2012). qRT-PCR analysis showed that both genes encoding PR1a and PDF1.2b were constitutively overexpressed in *map65-3*, when compared with the Wt (Fig. 5A). Upon infection with *Hpa*, *PR1* transcript levels increased more strongly in *map65-3* than in the Wt, whereas the amount of mRNA encoding PDF1.2b was reduced in the mutant when compared with the Wt (Fig. 5B, 5C). Interestingly, the overexpression of defense-related genes in *map65-3* was only observed in aerial parts of the plant, and was never detected in roots. In the absence of inoculation, *PR1a* and *PDF1.2b* transcripts were barely detectable in roots by qRT-PCR (Ct values >36.5 and 34.5, respectively).

These results suggested a role for AtMAP65-3 in the regulation of plant defense responses, and that gain of defense was responsible for the interaction phenotype of the mutant. This suggestion was confirmed by full-genome transcriptome analyses using Affymetrix ATH1 microarrays, in which we compared the responses that occurred 3 dai with *Hpa* or water treatment between the *map65-3* mutant and Wt plants (Fig. 6A). The direct comparison between water-treated plants from the Wt and the mutant (comparison a1, Fig. 6B) revealed that 152 and 76 genes were constitutively up- and down-regulated, respectively, in *map65-3* with a $\log_2$ ratio >1 (Supplementary Tables S2, S3). The direct comparison between *Hpa*-inoculated plants from the Wt and the mutant (comparison a2, Fig. 6B) showed that a further 302 and 52 genes were up- and down-regulated, respectively, in an infection-responsive manner in *map65-3* (Supplementary Tables S4, S5). Overall, 454 and 128 genes were at least 2-fold ($\log_2$ ratio >1) up- and down-regulated in the mutant, respectively, when compared with the Wt (Fig. 6B). We then compared the infection responsiveness between the mutant and Wt transcriptomes (Fig. 6A, C, comparison b1 with b2). While *Hpa* infection up- and down-regulates 394 and 20 genes in the Wt, the same treatment up- and down-regulates 739 and 71 genes in the mutant, respectively, with a $\log_2$ ratio >1 (Fig. 6C). When the expression ratio between *Hpa*-infected and water-treated Wt plants was subtracted from the expression ratio between *Hpa*-infected and water-treated mutant plants, 191 and 36 genes had 2-fold stronger up- and down-regulation ratios in *map65-3* (Supplementary Tables S6, S7). We submitted these genes to GO assignments (Katari *et al.*, 2010) for the term 'Biological Process'. We found that a significant over-represented number of genes involved in SA-associated defenses, including those involved in SA synthesis, signaling (*ICS1*, *SARD1*, *PAD4*, *NIMIN1*, and *EDS5*), and responsiveness (*PR1*, *PAD3*, chitinases, and glucanases) (Shah, 2003), were up-regulated in the mutant. In contrast, a significant over-represented number of JA-responsive genes (*PDF1.2b* or *PR4*) (Glazebrook, 2005) were down-regulated in *map65-3* (Fig. 6; Supplementary Tables S8, S9). These findings support that the mutation in *AtMAP65-3* accounts for a strong induction of SA-dependent defenses, and for the antagonistic inhibition of JA-dependent responses.

Gain of defense, but not map65-3*-associated dwarfism, depends on SA*

To confirm that up-regulated SA-dependent responses were responsible for reduced susceptibility of *map65-3*, we first determined the levels of free SA and its glycosylated storage form SAG in *map65-3*, following or not the infection with *Hpa*. Both SA and SAG were 2.5-fold more abundant in uninfected *map65-3* plants when compared with the Wt (Fig. 7A). Following infection with *Hpa* (3 dai), SA and SAG accumulated to >10-and 4-fold higher concentrations, respectively, in *map65*-3 than in the Wt (Fig. 7A). The increased accumulation was restored to Wt levels in the complemented mutant (Fig. 7A). These results strongly correlate with our transcriptomics data, and further suggest that decreased susceptibility of *map65-3* to filamentous biotrophs is governed by up-regulated SA synthesis and accumulation.

To confirm this statement, we generated a line (*map65-3/NahG×sid2.1*), in which SA signaling is completely abolished. We crossed the *map65-3* mutant expressing the bacterial *NahG* gene encoding salicylate hydroxylase, which converts SA to catechol thus preventing its accumulation (Delaney

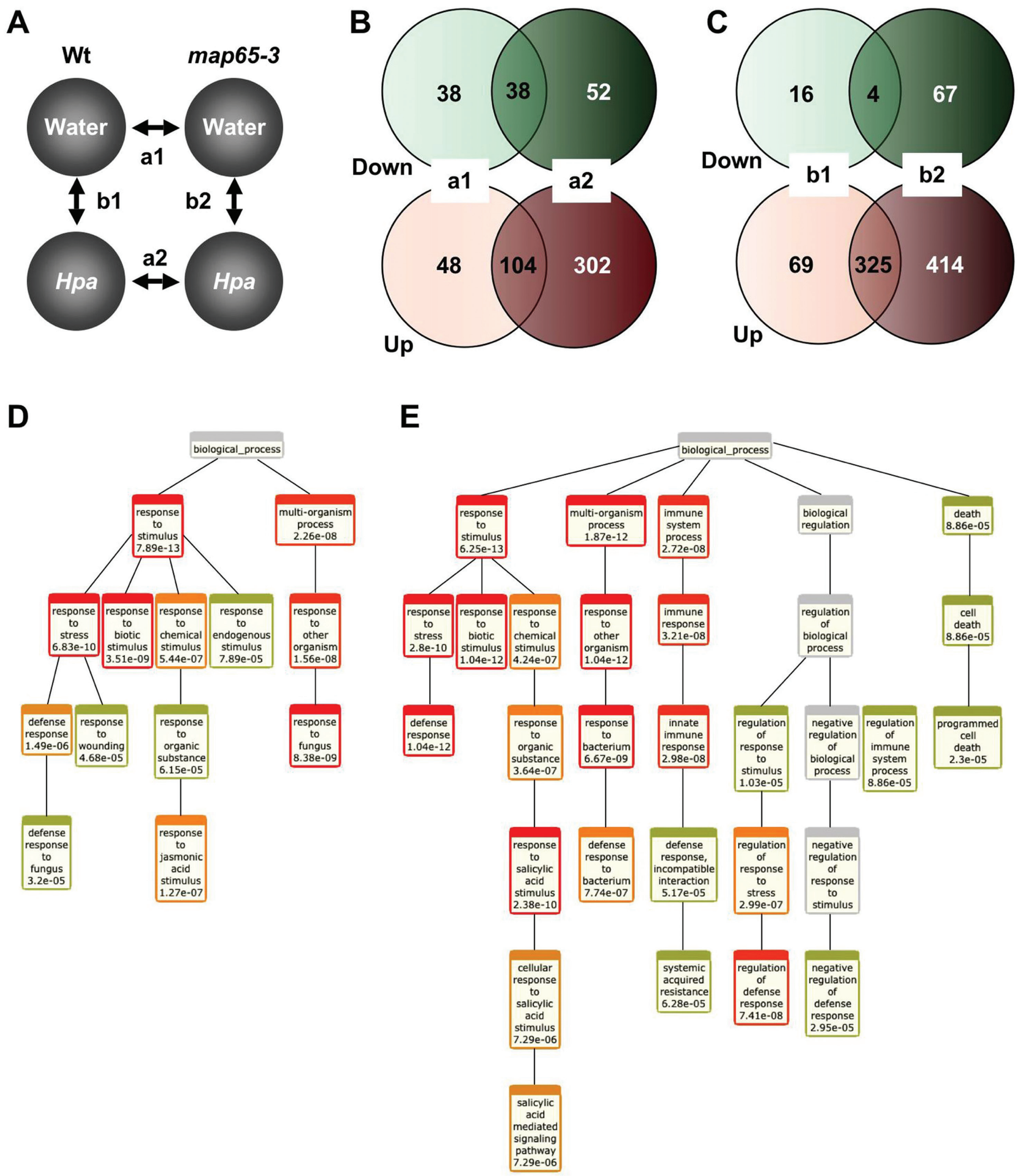

Fig. 6. The *map65-3* mutation significantly affects the plant transcriptome. (A–C) Comparison between Wt and *map65-3* mutant transcriptomes 3 d after treatment with water or inoculation with *Hpa*. (A) Schematic representation of the experimental design. Venn diagrams show *map65-3* vs WT (B) and infection-related (C) differences between genotypes. Genes were considered as differentially regulated when mean $\log_2$ signal ratios were ≥1 or ≤ –1. Functional classifications were performed using the VirtualPlant 1.3 online analysis tool (Katari *et al.*, 2010), for which the *A. thaliana* Tair10 ATH1 background with 20 969 unambiguous probes, the TAIR/TIGR GO Biological Process assignments, and the Fisher Exact Test with a *P*-value cut-off set to <0.0001 were taken into consideration. (D) An over-represented number of JA-responsive genes are less expressed in *map65-3*. (E) An over-represented number of genes involved in SA-associated defenses are more expressed in *map65-3*. (This figure is available in colour at *JXB* online.)

et al., 1994), with a *sid2-1* mutant impaired in SA biosynthesis (Nawrath and Métraux, 1999). qRT-PCR analysis for *PR1a* transcripts showed that the *map65-3*-dependent overexpression of the SA marker gene is absent from the *map65-3*/*NahG*×*sid2-1* line (Supplementary Fig. S2). Plants from the Wt, the *map65-3* mutant, and the SA-deficient *map65-3* mutant line were then analyzed for their susceptibility to the *Hpa* isolate Waco9. A strong reduction in *Hpa* sporulation (>50%) in the *map65-3* background was confirmed following inoculation of Arabidopsis leaves (Fig. 7B). Preventing SA synthesis and accumulation fully rescued *map65-3* susceptibility to *Hpa* (Fig. 7B).

Aberrant SA accumulation and the constitutive activation of defense affect plant growth (Huot *et al.*, 2014). We thus analyzed whether the described dwarf phenotype of *map65-3* (Caillaud *et al.*, 2008a) is a direct consequence of SA

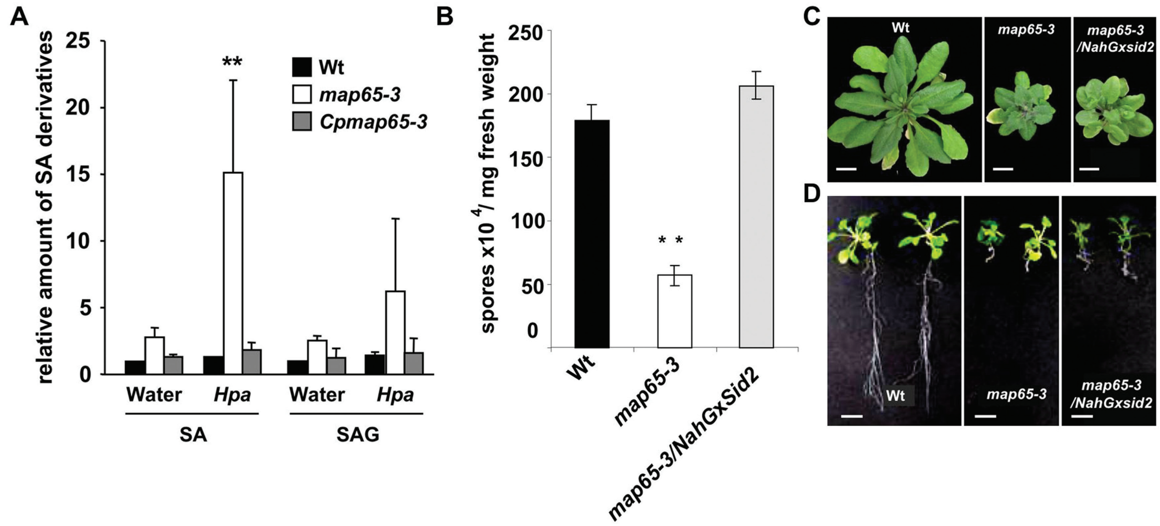

Fig. 7. SA accumulation in *map65-3* is responsible for decreased susceptibility to *Hpa*, but not for dwarfism. (A) Accumulation of salicylic acid (SA) and of the salicylic acid 2-O-β-glucoside (SAG) in cotyledons of the Wt (WS-4), the *map65-3* mutant, and the complemented line (*Cpmap65-3*), 3 d after treatment with water, or inoculation with the *Hpa* isolate Emwa1. The amounts of SA and SAG in the water-treated Wt were set to 1, corresponding to 8 ng of SA and 500 ng of SAG per gram of cotyledon fresh weight, respectively. Data are means ±SD from two biological replicates (B) Conidiospore production on rosettes of the Wt (WS×Col0), of the *map65-3* mutant (*map65-3*×Col0), and on the *map65-3/NahG*×*sid2.1* line. The bars represent mean values ±SE for 20 samples. Asterisks indicate a significant difference (*t*-test, P<0.01). Phenotypes of 8-week-old rosettes (C) and 4-week-old (D) roots from the Wt, the *map65-3* mutant, and the *map65-3/NahG*×*sid2.1* line. Scale bars=1 cm (C) and 0.2 cm (D).

accumulation and defense activation. The abolishment of SA synthesis and signaling was unable to rescue the dwarf phenotype of the *map65-3* mutant, and plants from the *map65-3/NahG*×*sid2-1* line exhibited smaller rosettes (Fig. 7C) and shorter roots (Fig. 7D), when compared with the Wt. It is noteworthy that the *map65-3/NahG*×*sid2* line showed similar susceptibility to *Hpa* as the Wt control despite this dwarf phenotype. Increased SA accumulation and defense signaling thus cause mildew resistance of *map65-3* mutants, but not the developmental phenotype, which was associated with a defect in cytokinesis (Müller *et al.*, 2004; Caillaud *et al.*, 2008b).

Discussion

We show that *AtMAP65-3* promoter activity is induced upon infection with *Hpa* and *Ec*, and that disruption of the *AtMAP65-3* gene decreases susceptibility to these biotrophic pathogens. Obligate biotrophic leaf pathogens, such as *Hpa* and *Ec*, are successful in colonizing plant tissues only when they are able to avoid defense responses and to reprogram the host for nutrient supply. Both *Hpa* and *Ec* must establish haustoria to withdraw nutrients and water from host cells and to sustain growth of hyphae and reproduction. Haustoria formation in host plant cells requires a rapid growth of membrane surfaces and the creation of the extrahaustorial matrix, a new apoplastic compartment (O'Connell and Panstruga, 2006). As previous studies demonstrated the implication of MTs of the host cell in the development of intracellular structures induced by biotrophs (Schmidt and Panstruga, 2007; Hoefle *et al.*, 2011; Hardham, 2013), we investigated whether AtMAP65-3 contributes to the reorganization of MTs in cells bearing haustoria of *Hpa* and *Ec*. Using GFP–TUA6 fusions, we confirmed that MT restructuring is associated with *Hpa* haustoria development, and that MT arrays encase the oomycete feeding site. MT reorganization was also observed at *Ec* penetration sites in Arabidopsis epidermal cells, as described previously for *Blumeria graminis* in barley (Kobayashi *et al.*, 1994; Hoefle *et al.*, 2011). However, the presence or absence of AtMAP65-3 did not obviously influence MT dynamics during *Hpa* and *Ec* invasion and haustoria development. AtMAP65-3 plays a critical role during assembly of mitotic MT arrays and during cytokinesis in dividing cells from roots and shoots (Müller *et al.*, 2004; Caillaud *et al.*, 2008*b*). We did not find such a function for AtMAP65-3 in MT bundling in non-dividing plant cells, such as haustoria-harboring cells from cotyledons or leaves, which are colonized by *Hpa* and *Ec*. It is thus unlikely that AtMAP65-3 directly serves the demands of the pathogens during haustorium formation or nutrient acquisition. Our findings show rather that AtMAP65-3 plays a role as a negative regulator of defenses against cell wall penetration by filamentous pathogens and post-penetration defense gene expression.

Defense-related genes are mostly down-regulated during the early steps of compatible, biotrophic interactions between Arabidopsis and oomycetes or fungi (Chandran *et al.*, 2009; Hok *et al.*, 2011). Here, we demonstrate that *map65-3* mutants accumulate SA, and that they are primed for enhanced defenses against biotrophic leaf pathogens. We thus conclude that AtMAP65-3 negatively regulates SA-dependent plant immunity, and that *Hpa* and *Ec* activate the transcription of *AtMAP65-3* to repress plant defenses and promote infection.

Mutants with constitutively activated SA-dependent defenses often show a dwarf phenotype (Huot *et al.*, 2014; Janda and Ruelland, 2014). The association of constitutive defense activation with dwarfism is subject to discussion. It might result from the reallocation of resources for growth and reproduction to SA-mediated responses (Heidel *et al.*, 2004), or be a direct consequence of the repression of auxin signaling by antagonistic SA (Naseem *et al.*, 2015). However, our studies show that dwarfism of the *map65-3* mutant is not a consequence of aberrant SA accumulation and defense activation, as eliminating SA from the mutants restores Wt susceptibility, but not Wt growth. AtMAP65-3 thus has either independent roles for cytokinesis and defense activation, or SA accumulation and defense activation are a consequence of cytokinesis defects. A prominent example for a protein involved in the regulation of both the cell cycle and plant immunity is constitutive pathogen response5, CPR5 (Bowling *et al.*, 1997; Kirik *et al.*, 2001; Yoshida *et al.*, 2002). Like *map65-3*, *cpr5* mutants are constitutively activated for defense responses, and show a dwarf phenotype. Similar to what we found for *map65-3*, blocked SA accumulation in *cpr5* suppresses the disease resistance phenotype, but not the stunted growth morphology, thus placing *cpr5* either upstream of SA synthesis, or independent from it (Wang *et al.*, 2014). CPR5 is a nuclear envelope protein and associates with the cyclin-dependent kinase inhibitors (CKIs), SIAMESE (SIM) and SIAMESE-RELATED1 (SMR1). This association is essential for maintaining defense responses repressed in the normal (non-infected) state of Arabidopsis. When immune responses are triggered, the CKIs are released from CPR5 to cause overactivation of cell cycle regulators from the E2F family. *sim*, *smr1*, and *e2fabc* mutants are compromised in immune responses, showing that CPR5 acts upstream of SA, and indicating that the CKIs and E2Fs constitute functional links between CPR5 and downstream SA signaling (Wang *et al.*, 2014). It is noteworthy that the *map65-3* mutation does not affect the transcriptional regulation of *SIM*, *SMR1*, and *E2Fa*, *b*, and *c* (compare Supplementary Tables S2–S7), suggesting that MAP65-3 interferes with SA-mediated defenses independent of these regulators of the cell cycle signaling pathway.

MAPKs are essential for innate immune signal transduction (Zipfel *et al.*, 2004). There is growing evidence that MAPKs also regulate the activity of MAP65 proteins (Komis *et al.*, 2011; Šamajová *et al.*, 2013), and AtMAP65-3 was shown to be a substrate for the MAPK, AtMPK4 (Kosetsu *et al.*, 2010; Beck *et al.*, 2011; Sasabe *et al.*, 2011). Similar to *map65-3*, *mpk4* mutants show defects in cytokinesis, and have a stunted growth phenotype (Kosetsu *et al.*, 2010; Beck *et al.*, 2011). In addition, AtMPK4 negatively regulates plant defense responses, and *mpk4* mutants accumulate increased amounts of SA (Petersen *et al.*, 2000; Brodersen *et al.*, 2006). The absence of MPK4 from Arabidopsis and soybean leads to enhanced penetration resistance to filamentous pathogens (Petersen *et al.*, 2000; Liu *et al.*, 2011). Also similar to what we show for *map65-3*, the growth defect of *mpk4* mutants is independent of SA accumulation (Gawroński *et al.*, 2014). Further studies have to show whether AtMAP65-3 is a substrate for AtMPK4 in a signaling cascade, which determines both cytokinesis and pathogen defense.

The dwarf phenotype of *map65-3*, which is independent of SA accumulation, might be explained by the mitotic and cytokinetic defects previously described for this mutant (Müller *et al.*, 2004; Caillaud *et al.*, 2008*b*). We show that SA signaling and *PR1* transcript accumulations are induced in leaves and cotyledons of the *map65-3* mutant, but not in roots. A difference between shoots and roots with respect to SA-mediated signal transduction has previously been reported for other SA-accumulating Arabidopsis mutants such as *cpr1* (affected in an F-Box protein that targets resistance proteins and negatively regulates defense responses; Wubben *et al.*, 2008) or *pi4kIIIβ1β2* (phosphatidylinositol-4-kinases; Šašek *et al.*, 2014). Differences between shoots and roots in perception and response to SA remain, however, unexplained.

The role of MTs in induced plant immunity most probably relies on their action in driving vesicular trafficking, allowing host-secreted molecules (e.g. cell wall components, antimicrobial molecules, or callose) to accumulate in the extracellular space and to contribute to the control of plant invasion by pathogens (Hardham, 2013). MTs and MAPs probably also participate in the earlier responses to biotic factors that are initiated at the plasma membrane, downstream of PAMP perception. As an example, the phospholipases D (PLDs), that bind to cortical MTs, and the PLD-derived phosphatidic acid (PA) play a key role in early steps leading to defense responses (Zhao, 2015). PLDs and PLDα1-derived PA were shown to bind to cortical MTs and MAP65-1, respectively, thus regulating MT polymerization and bundling under salt stress (Dhonukshe *et al.*, 2003; Zhang *et al.*, 2012). Pharmacological attempts to destabilize MT assembly often alter plant susceptibility to pathogens (reviewed by Hardham, 2013). In barley, ROP GTPase-regulated MT reorganization is involved in penetration resistance and susceptibility to invasion by the powdery mildew fungus *Blumeria graminis* f.sp. *hordei* (Hoefle *et al.*, 2011; Dörmann *et al.*, 2014). Some pathogen-secreted effectors also target MTs for suppressing host defenses. Examples are the effectors HopZ1a and AvrBST from the phytopathogenic bacteria *Pseudomonas syringae* and *Xanthomonas campestris*, respectively. HopZ1a is an acetyltransferase that binds and acetylates plant tubulin, thus causing the destruction of MTs, the inhibition of secretory pathways, and the suppression of plant defenses (Lee *et al.*, 2012). AvrBsT targets and acetylates Acetylated Interacting Protein1 (ACIP1), a cortical MT-associated protein. ACIP1 acetylation alters its localization and its function in plant defense against bacteria (Cheong *et al.*, 2014). Further research will be necessary to understand how the MT cytoskeleton and AtMAPs, including AtMAP65-3, participate in the signal transduction pathways that connect pathogen perception to the activation of immune responses. Further research will be necessary to understand how the MT cytoskeleton and MAPs participate in the signal transduction pathways that connect pathogen perception to the activation of immune responses, and how AtMAP65-3 mediates the balance between development and immunity in plants. The identification of additional regulatory modules that interact with AtMAP65-3, and probably involve AtMPK4, will certainly help in understanding molecular signaling switches that are engaged during developmental processes and immune responses.

Supplementary data

Supplementary data are available at *JXB* online.

Table S1. Oligonucleotides used in this study.

Table S2. Genes that are constitutively more expressed in *map65-3* than in the Wt (≥2-fold).

Table S3. Genes that are constitutively less expressed in *map65-3* than in the Wt (≥2-fold).

Table S4. Genes that are more expressed in *map65-3* than in the Wt upon *Hpa* infection (≥2-fold).

Table S5. Genes that are less expressed in *map65-3* than in the Wt upon *Hpa* infection (≥2-fold).

Table S6. Infection-responsive genes that are ≥2-fold more expressed in *map65-3* than in the Wt.

Table S7. Infection-responsive genes that are ≥2-fold less expressed in *map65-3* than in the Wt.

Table S8. Over-represented genes that are ≥2-fold more expressed in *map65-3* than in the Wt upon infection.

Table S9. Over-represented genes that are ≥2-fold less expressed in *map65-3* than in the Wt upon infection.

Figure S1. Morphogenesis of *Hpa* haustoria is not affected in the *map65-3* mutant.

Figure S2. Relative gene expression of *PR1a* and *PDF1.2b* in shoots of the Wt (WS×Col0), of the *map65-3* mutant (*map65-3*×Col0), and on the *map65-3*/*NahG*×*sid2.1* line.

Acknowledgements

The construct carrying the *35S::NahG* construction was a kind gift from Dr L'Haridon (Fribourg University). The *sid2.1* and GFP–TUA6 were kindly provided by Dr A. Attard (INRA Sophia Antipolis, France) and Dr Hashimoto (Nara, Japan), respectively. We thank Benoit Industri and Michel Ponchet (INRA Sophia Antipolis, France) for providing an SA quantification protocol, and discussing the results. This work was supported by INRA and by the French Government (National Research Agency, ANR) through the 'Investments for the Future' LABEX SIGNALIFE [program reference #ANR-11-LABX-0028-01], by the ANR/Génoplante program SCRIPS [ANR-08-GENM-014], and by the German Research Foundation [grant number #DFG FOR666, #DFG SFB924]. MCC received support from an MC FP7-PEOPLE-2009-IEF fellowship and BBSRC-UK grant [BB/K009176/1].

References

Baluska F, Bacigalova K, Oud JL, Hauskrecht M, Kubica S. 1995. Rapid reorganization of microtubular cytoskeleton accompanies early changes in nuclear ploidy and chromatin structure in postmitotic cells of barley leaves infected with powdery mildew. Protoplasma **185,** 140–151.

Beck M, Komis G, Ziemann A, Menzel D, Samaj J. 2011. Mitogen-activated protein kinase 4 is involved in the regulation of mitotic and cytokinetic microtubule transitions in Arabidopsis thaliana. New Phytologist **189,** 1069–1083.

Bowling SA, Clarke JD, Liu Y, Klessig DF, Dong X. 1997. The cpr5 mutant of Arabidopsis expresses both NPR1-dependent and NPR1-independent resistance. The Plant Cell **9,** 1573–1584.

Brodersen P, Petersen M, Bjørn Nielsen H, Zhu S, Newman M-A, Shokat KM, Rietz S, Parker J, Mundy J. 2006. Arabidopsis MAP kinase 4 regulates salicylic acid- and jasmonic acid/ethylene-dependent responses via EDS1 and PAD4. The Plant Journal **47,** 532–546.

Cahill D, Rookes J, Michalczyk A, McDonald K, Drake A. 2002. Microtubule dynamics in compatible and incompatible interactions of soybean hypocotyl cells with Phytophthora sojae. Plant Pathology **51,** 629–640.

Cai G, Faleri C, Del Casino C, Emons AMC, Cresti M. 2011. Distribution of callose synthase, cellulose synthase, and sucrose synthase in tobacco pollen tube is controlled in dissimilar ways by actin filaments and microtubules. Plant Physiology **155,** 1169–1190.

Caillaud MC, Abad P, Favery B. 2008*a*. Cytoskeleton reorganization, a key process in root-knot nematode-induced giant cell ontogenesis. Plant Signaling and Behavior **3,** 816–818.

Caillaud MC, Lecomte P, Jammes F, *et al.* 2008*b*. MAP65-3 microtubule-associated protein is essential for nematode-induced giant cell ontogenesis in Arabidopsis. The Plant Cell **20,** 423–427.

Caillaud MC, Piquerez SJM, Fabro G, Steinbrenner J, Ishaque N, Beynon J, Jones JDG. 2012. Subcellular localization of the *Hpa* RxLR effector repertoire identifies a tonoplast-associated protein HaRxL17 that confers enhanced plant susceptibility. The Plant Journal **69,** 252–265.

Chan J, Jensen CG, Jensen LC, Bush M, Lloyd CW. 1999. The 65-kDa carrot microtubule-associated protein forms regularly arranged filamentous cross-bridges between microtubules. Proceedings of the National Academy of Sciences, USA **96,** 14931–14936.

Chandran D, Tai YC, Hather G, Dewdney J, Denoux C, Burgess DG, Ausubel FM, Speed TP, Wildermuth MC. 2009. Temporal global expression data reveal known and novel salicylate-impacted processes and regulators mediating powdery mildew growth and reproduction on Arabidopsis. Plant Physiology **149,** 1435–1451.

Cheong MS, Kirik A, Kim J-G, Frame K, Kirik V, Mudgett MB. 2014. AvrBsT acetylates Arabidopsis ACIP1, a protein that associates with microtubules and is required for immunity. PLoS Pathogens **10,** e1003952.

Clough SJ, Bent AF. 1998. Floral dip: a simplified method for Agrobacterium-mediated transformation of Arabidopsis thaliana. The Plant Journal **16,** 735–743.

Dangl JL, Horvath DM, Staskawicz BJ. 2013. Pivoting the plant immune system from dissection to deployment. Science **341,** 746–751.

De Almeida Engler J, Favery B. 2011. The plant cytoskeleton remodelling in nematode induced feeding sites. In: Jones J, Gheysen G, Fenoll C, eds. Genomics and molecular genetics of plant–nematode interactions . Heidelberg: Springer, 369–393.

De Almeida Engler J, Favery B, Engler G, Abad P. 2005 Loss of susceptibility as an alternative for nematode resistance. Current Opinion in Biotechnology **16,** 112–117.

Delaney TP, Uknes S, Vernooij B, *et al.* 1994. A central role of salicylic acid in plant disease resistance. Science **266,** 1247–1250.

Dhonukshe P, Laxalt AM, Goedhart J, Gadella TW, Munnik T. 2003. Phospholipase D activation correlates with microtubule reorganization in living plant cells. The Plant Cell **15,** 2666–2679.

Dörmann P, Kim H, Ott T, Schulze-Lefert P, Trujillo M, Wewer V, Hückelhoven R. 2014. Cell-autonomous defense, re-organization and trafficking of membranes in plant–microbe interactions. New Phytologist **204,** 815–822.

Ellinger D, Voigt CA. 2014. Callose biosynthesis in arabidopsis with a focus on pathogen response: what we have learned within the last decade. Annals of Botany **114,** 1349–1358.

Gardiner J. 2013. The evolution and diversification of plant microtubule-associated proteins. The Plant Journal **75,** 219–229.

Gawroński P, Witoń D, Vashutina K, Bederska M, Betliński B, Rusaczonek A, Karpiński S. 2014. Mitogen-activated protein kinase 4 is a salicylic acid-independent regulator of growth but not of photosynthesis in Arabidopsis. Molecular Plant **7,** 1151–1166.

Genre A, Chabaud M, Timmers T. 2005. Arbuscular mycorrhizal fungi elicit a novel intracellular apparatus in *Medicago truncatula* root epidermal cells before infection. The Plant Cell **17,** 3489–3499.

Glazebrook J. 2005. Contrasting mechanisms of defense against biotrophic and necrotrophic pathogens. Annual Review of Phytopathology **43,** 205–227.

Hamada T. 2014. Microtubule organization and microtubule-associated proteins in plant cells. International Review of Cell and Molecular Biology **312,** 1–52.

Hardham AR. 2013. Microtubules and biotic interactions. The Plant Journal **75,** 278–289.

Hardham AR, Takemoto D, White RG. 2008. Rapid and dynamic subcellular reorganization following mechanical stimulation of Arabidopsis epidermal cells mimics responses to fungal and oomycete attack. BMC Plant Biology **8,** 63.

Heidel AJ, Clarke JD, Antonovics J, Dong X. 2004. Fitness costs of mutations affecting the systemic acquired resistance pathway in Arabidopsis thaliana. Genetics **168,** 2197–2206.

Hellemans J, Mortier G, De Paepe A, Speleman F, Vandesompele J. 2007. qBase relative quantification framework and software for management and automated analysis of real-time quantitative PCR data. Genome Biology **8,** R19.

Ho C-MK, Hotta T, Guo F, Roberson RW, Lee Y-RJ, Liu B. 2011. Interaction of antiparallel microtubules in the phragmoplast is mediated by the microtubule-associated protein MAP65-3 in Arabidopsis. The Plant Cell **23,** 2909–2923.

Hoefle C, Huesmann C, Schultheiss H, Börnke F, Hensel G, Kumlehn J, Hückelhoven R. 2011. A barley ROP GTPase ACTIVATING PROTEIN associates with microtubules and regulates entry of the barley powdery mildew fungus into leaf epidermal cells. The Plant Cell **23,** 2422–2439.

Hok S, Danchin EGJ, Allasia V, Panabières F, Attard A, Keller H. 2011. An Arabidopsis (malectin-like) leucine-rich repeat receptor-like kinase contributes to downy mildew disease. Plant, Cell and Environment **34,** 1944–1957.

Hückelhoven R, Eichmann R, Weis C, Hoefle C, Proels RK. 2013. Genetic loss of susceptibility: a costly route to disease resistance? Plant Pathology **62,** 56–62.

Huot B, Yao J, Montgomery BL, He SY. 2014. Growth–defense tradeoffs in plants: a balancing act to optimize fitness. Molecular Plant **7,** 1267–1287.

Hussey PJ, Hawkins TJ, Igarashi H, Kaloriti D, Smertenko A. 2002. The plant cytoskeleton: recent advances in the study of the plant microtubule-associated proteins MAP-65, MAP-190 and the Xenopus MAP215-like protein, MOR1. Plant Molecular Biology **50,** 915–924.

Jacobs AK, Lipka V, Burton RA, Panstruga R, Strizhov N, Schulze-Lefert P, Fincher GB. 2003. An Arabidopsis callose synthase, GSL5, is required for wound and papillary callose formation. The Plant Cell **15,** 2503–2513.

Janda M, Ruelland E. 2014. Magical mystery tour: salicylic acid signalling. Environmental and Experimental Botany **114,** 117–128.

Jones JDG, Dangl JL. 2006. The plant immune system. Nature **444,** 323–329.

Katari MS, Nowicki SD, Aceituno FF, *et al.* 2010. VirtualPlant: a software platform to support systems biology research . Plant Physiology **152,** 500–515.

Kirik V, Bouyer D, Schobinger U, Bechtold N, Herzog M, Bonneville JM, Hülskamp M. 2001. CPR5 is involved in cell proliferation and cell death control and encodes a novel transmembrane protein. Current Biology **11,** 1891–1895.

Kobayashi I, Kobayashi Y, Hardham AR. 1994. Dynamic reorganization of microtubules and microfilaments in flax cells during the resistance response to flax rust infection. Planta **61,** 237–247.

Koch E, Slusarenko A. 1990. Arabidopsis is susceptible to infection by a downy mildew fungus. The Plant Cell **2,** 437–445.

Komis G, Illés P, Beck M, Šamaj J. 2011. Microtubules and mitogen-activated protein kinase signalling. Current Opinion in Plant Biology **14,** 650–657.

Kosetsu K, Matsunaga S, Nakagami H, Colcombet J, Sasabe M, Soyano T, Takahashi Y, Hirt H, Machida Y. 2010. The MAP kinase MPK4 is required for cytokinesis in Arabidopsis thaliana. The Plant Cell **22,** 3778–3790.

Kragler F, Curin M, Trutnyeva K, Gansch A, Waigmann E. 2003. MPB2C, a microtubule-associated plant protein binds to and interferes with cell-to-cell transport of tobacco mosaic virus movement protein. Plant Physiology **132,** 1870–1883.

Lapin D, Van den Ackerveken G. 2013. Susceptibility to plant disease: more than a failure of host immunity. Trends in Plant Sciences **18,** 546–554.

Lee AHY, Hurley B, Felsensteiner C, *et al.* 2012. A bacterial acetyltransferase destroys plant microtubule networks and blocks secretion. PLoS Pathogens **8,** e1002523.

Liu J-Z, Horstman HD, Braun E, *et al.* 2011. Soybean homologs of MPK4 negatively regulate defense responses and positively regulate growth and development. Plant Physiology **157,** 1363–1378.

Martinière A, Gargani D, Uzest M, Lautredou N, Blanc S, Drucker M. 2009. A role for plant microtubules in the formation of transmission-specific inclusion bodies of Cauliflower mosaic virus. The Plant Journal **58,** 135–146.

Meuwly P, Métraux JP. 1993. Ortho-anisic acid as internal standard for the simultaneous quantitation of salicylic acid and its putative biosynthetic precursors in cucumber leaves. Analytical Biochemistry **214,** 500–505.

Mucha E, Fricke I, Schaefer A, Wittinghofer A, Berken A. 2011. Rho proteins of plants—functional cycle and regulation of cytoskeletal dynamics. European Journal of Cell Biology **90,** 934–943.

Müller S, Smertenko A, Wagner V, Heinrich M, Hussey PJ, Hauser MT. 2004. The plant microtubule-associated protein AtMAP65-3/PLE is essential for cytokinetic phragmoplast function. Current Biology **14,** 412–417.

Naseem M, Kaltdorf M, Dandekar T. 2015. The nexus between growth and defence signalling: auxin and cytokinin modulate plant immune response pathways. Journal of Experimental Botany **66,** 4885–4896.

Nawrath C, Métraux JP. 1999. Salicylic acid induction-deficient mutants of Arabidopsis express PR-2 and PR-5 and accumulate high levels of camalexin after pathogen inoculation. The Plant Cell **11,** 1393–1404.

Nishimura MT, Stein M, Hou B-H, Vogel JP, Edwards H, Somerville SC. 2003. Loss of a callose synthase results in salicylic acid-dependent disease resistance. Science **301,** 969–972.

O'Connell RJ, Panstruga R. 2006. Tête à tête inside a plant cell: establishing compatibility between plants and biotrophic fungi and oomycetes. New Phytologist **171,** 699–718.

Ouko MO, Sambade A, Brandner K, Niehl A, Peña E, Ahad A, Heinlein M, Nick P. 2010. Tobacco mutants with reduced microtubule dynamics are less susceptible to TMV. The Plant Journal **62,** 829–839.

Parker JE, Coleman MJ, Szabo V, Frost LN, Schmidt R, van der Biezen EA, Moores T, Dean C, Daniel MJ, Jones JGD. 1997. The Arabidopsis downy mildew resistance gene RPP5 shares similarity to the toll and interleukin-1 receptors with N and L6. The Plant Cell **8,** 2033–2046.

Petersen M, Brodersen P, Naested H, *et al.* 2000. Arabidopsis map kinase 4 negatively regulates systemic acquired resistance. Cell **103,** 1111–1120.

Pieterse CMJ, Van der Does D, Zamioudis C, Leon-Reyes A, Van Wees SCM. 2012. Hormonal modulation of plant immunity. Annual Review of Cell and Developmental Biology **28,** 489–521.

Poraty-Gavra L, Zimmermann P, Haigis S, Bednarek P, Hazak O, Stelmakh OR, Sadot E, Schulze-Lefert P, Gruissem W, Yalovsky S. 2013. The Arabidopsis Rho of plants GTPase AtROP6 functions in developmental and pathogen response pathways. Plant Physiology **161,** 1172–1188.

Quentin M, Allasia V, Pegard A, *et al.* 2009. Imbalanced lignin biosynthesis promotes the sexual reproduction of homothallic oomycete pathogens. PLoS Pathogens **5,** e1000264.

Šamajová O, Komis G, Šamaj J. 2013. Emerging topics in the cell biology of mitogen-activated protein kinases. Trends in Plant Science **18,** 140–148.

Sasabe M, Kosetsu K, Hidaka M, Murase A, Machida Y. 2011. Arabidopsis thaliana MAP65-1 and MAP65-2 function redundantly with MAP65-3/PLEIADE in cytokinesis downstream of MPK4. Plant Signaling and Behavior **6,** 743–747.

Šašek V, Janda M, Delage E, *et al.* 2014. Constitutive salicylic acid accumulation in pi4kIIIβ1β2 Arabidopsis plants stunts rosette but not root growth. New Phytologist **203,** 805–816.

Schmidt SM, Panstruga R. 2007. Cytoskeleton functions in plant–microbe interactions. Physiological and Molecular Plant Pathology **71,** 135–148.

Shah J. 2003. The salicylic acid loop in plant defense. Current Opinion in Plant Biology **6,** 365–371.

Takemoto D, Hardham AR. 2004. The cytoskeleton as a regulator and target of biotic interactions in plants. Plant Physiology **136,** 3864–3876.

Takemoto D, Jones DA, Hardham AR. 2003. GFP-tagging of cell components reveals the dynamics of subcellular re-organization in response to infection of Arabidopsis by oomycete pathogens. The Plant Journal **33,** 775–792.

Ueda K, Matsuyama T, Hashimoto T. 1999. Visualization of microtubules in living cells of transgenic Arabidopsis thaliana. Protoplasma **206,** 201–206.

Van Schie CC, Takken FL. 2014. Susceptibility genes: how to be a good host. Annual Reviews of Phytopathology , **52,** 551–581.

Vassileva VN, Kouchi H, Ridge RW. 2005. Microtubule dynamics in living root hairs: transient slowing by lipochitin oligosaccharide nodulation signals. The Plant Cell **17,** 1777–1787.

Wang S, Gu Y, Zebell SG, Anderson LK, Wang W, Mohan R, Dong X. 2014. A noncanonical role for the CKI–RB–E2F cell-cycle signaling pathway in plant effector-triggered immunity. Cell Host and Microbe **16,** 787–794.

Wasteneys GO. 2004. Progress in understanding the role of microtubules in plant cells. Current Opinion in Plant Biology **7,** 651–660.

Wasteneys GO, Galway ME. 2003. Remodeling the cytoskeleton for growth and form: an overview with some new views. Annual Review of Plant Biology **54,** 691–722.

Wubben MJE, Jin J, Baum TJ. 2008. Cyst nematode parasitism of Arabidopsis thaliana is inhibited by salicylic acid (SA) and elicits uncoupled SA-independent pathogenesis-related gene expression in roots. Molecular Plant Microbe Interactions **21,** 424–432.

Yoshida S, Ito M, Nishida I, Watanabe A. 2002. Identification of a novel gene HYS1/CPR5 that has a repressive role in the induction of leaf senescence and pathogen-defence responses in Arabidopsis thaliana. The Plant Journal **29,** 427–437.

Yeh Y-H, Chang Y-H, Huang P-Y, Huang J-B, Zimmerli L. 2015. Enhanced Arabidopsis pattern-triggered immunity by overexpression of cysteine-rich receptor-like kinases. Frontiers in Plant Science **6,** 322.

Zhang Q, Lin F, Mao T, Nie J, Yan M, Yuan M, Zhang W. 2012. Phosphatidic acid regulates microtubule organization by interacting with MAP65-1 in response to salt stress in Arabidopsis. The Plant Cell **24,** 4555–4576.

Zhao J. 2015. Phospholipase D and phosphatidic acid in plant defence response: from protein–protein and lipid–protein interactions to hormone signalling. Journal of Experimental Botany **66,** 1721–1736.

Zipfel C, Robatzek S, Navarro L, Oakeley EJ, Jones JDG, Felix G, Boller T. 2004. Bacterial disease resistance in Arabidopsis through flagellin perception. Nature **428,** 764–767.